Adhesive Stresses in Wide Flange Steel Beams Bonded To GFRP Plate under Transverse Bending

Phe Van Pham and Magdi Mohareb
A120A, Colonel By building, Ottawa University, Ottawa, ON, Canada
ppham040@uottwa.ca; MagdiEmile.Mohareb@uottawa.ca

Abstract- The present study investigates the stress state in adhesive material bonding wide steel flange beams reinforced with GFRP plate and subjected to transverse bending. Based on a 3D finite element analysis, contour plots are obtained for the stress fields within the adhesive layer. The most predominant stress fields and locations of peak stresses are identified for typical beam geometries. A parametric study is then performed to investigate the effect of shear modulus of the adhesive layer, adhesive layer thickness, and GFRP plate thickness on the resulting maximum von Mises stress within adhesive layer and the transverse displacements. The study proposes practical measures to be taken to reduce stresses within the adhesive layer while ensuring effective composite action for steel beams under transverse bending.

1. Motivation and Scope

Relatively recently, GFRP plates have been considered as a retrofit technique for steel beams. GFRP plates are bonded to steel members through an adhesive layer. The limited number of experimental studies (e.g., El Damatty and Abushagur (2003) and Damatty et al. (2003)) on steel beams bonded to GFRP plates suggests that the capacity of such systems can be governed by the failure of the adhesive material either in a shearing mode or in a peeling mode. The present study aims at developing insight on the behaviour of steel beams bonded to GFRP plate through an adhesive layer when subjected to transverse bending. Emphasis is placed on stress distributions and magnitudes within the adhesive layer through a parametric study based on a 3D finite element model under Abaqus. Towards this goal, a review is provided of adhesive properties (Section 2). The paper defines two reference cases based on realistic geometric and material parameters (Section 3), modelled using 3D FEA (Section 4) and the important stress fields and distributions are identified (Section 5). Deviations from the reference case are then examined to develop insight on the effects of the shear modulus of the adhesive, the adhesive thickness, and the GFRP thickness (Section 6) on the stresses induced into the adhesive layer the induced midspan displacement.

2. Adhesive Properties

A summary of experimental work aimed at investigating the material properties of the adhesive is shown in Table 1. El Damatty and Abushagur (2003) showed that maximum shear stresses at interfaces of adhesive layer ranged from 20.9 to 34.3 MPa while the maximum peeling stresses ranged from 0.72 to 6.01 MPa. Xia and Teng (2005) observed that FRP-to-Steel composite structures with thin adhesive layer thicknesses (< 2mm) undergo adhesive failures. Schnerch (2005) performed a detailed study on the adhesives bonding FRP material to steel members.

Table 1. Mechanical properties of adhesive layer used in literature.

Authors	Adhesive Type	Tensile strength (MPa)	Young's Modulus (MPa)	Poisson's ratio	Ultimate tensile strain (%)
Miller et al. (2001)	AV8113/HV8113	13.8-17.2	107	-	-
	PlexusMA555	8.6-10.3	-	-	-
Damatty et al. (2003), (2013)	MA 420	15.5	-	-	-
Xia and Teng (2005)	A (CIBA)	22.53	4013	0.36	0.5614
	B (SIKA)	20.48	10793	0.27	0.1898
	C	13.89	5426	0.31	0.2560
Schnerch (2005)	SP Spabond	37.1	3007	0.38	0.0132
	SP spabond 345	34.6	3007	0.38	0.0132
Linghoff et al. (2010)	Epoxy 1	25	7000	-	-
	Epoxy 2	30	4500	-	-
Peiris (2011)	SP Spabond 345	34.6	3007	0.38	0.0132

3. Reference Cases

A 3m span simply supported $W310\times60$ steel beam is reinforced by a GFRP plate through an adhesive layer (Fig. 1). The GFRP plate has a thickness $t_p = 19mm$ and a width $b_p = 100mm$. Modulus of elasticity of steel is $E_s = 200GPa$, that of GFRP is $E_p = 42GPa$. Poisson's ratio μ for all three materials is taken as 0.3. Transversely, the wide flange beam is simply supported. Longitudinally, the end $z = 0$ of the beam axis is restrained while at $z = L$, it is axially free. Both ends of the GFRP plate are longitudinally free. The adhesive thickness is $t_a = 2mm$. The beam is subjected to a two concentrated loads $2 \times P/2 = 200kN$ applied at mid-span as shown. Two reference cases are considered to investigate the stress distributions within the adhesive layer, which are Reference case R1 where the adhesive shear modulus is taken as $G_a = 0.1GPa$ and the Reference case R2 where adhesive shear modulus is taken as $G_a = 0.4GPa$.
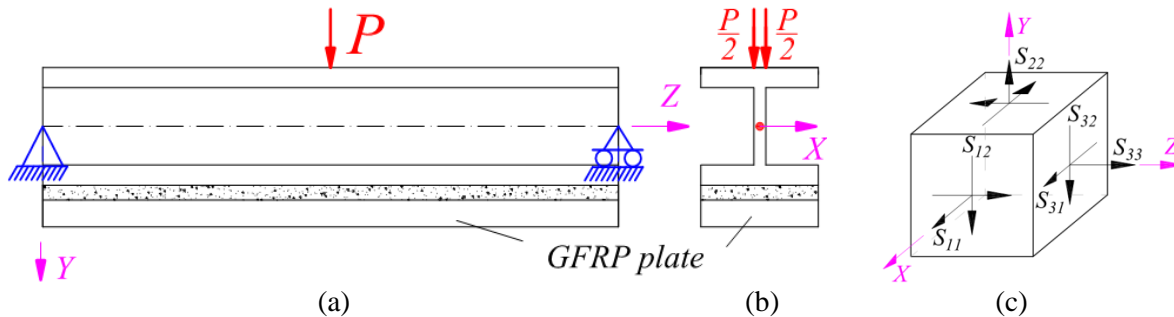

Fig. 1. Simply supported beam reinforced with GFRP plate (a) Elevation, (b) Tractions acting at tip inducing transverse bending and (c) Stress components of an element

4. Finite Element Model

The 3D FEA simulation is conducted using the 8-node brick element C3D8R from the ABAQUS library. The element has 24 degrees of freedom (with three translations at each of the eight nodes) and uses reduced integration to avoid volumetric locking. Thus, the element has a single integration point located at the element centroid. Boundary conditions are set up for nodes of two lateral lines passing the centroidal nodes of the first and last beam cross-sections. A mesh study (Pham and Mohareb 2014 a, b) indicated that convergence is achieved when using 15 elements along the flange half flange width excluding the web, 12 elements across the flange thickness, 50 elements along the web height, 4 elements across the web thickness, 4 elements across the adhesive thickness, 8 elements across the GFRP thickness, and 3120 elements in the longitudinal direction.

5. Stresses Within Adhesive

The "view cut" function in Abaqus CAE is used to obtain the stress contour plans at Steel-Adhesive (SA) and Adhesive-Plate (AP) interfaces (Figures 2 and 3). Different length scale factors (i.e., the scale factor in the direction of the lateral direction is taken as seven times larger than that in the longitudinal direction) for better visualization of the results in the contour plots. In reference case R1, of the six stress contours (Fig. 2a-f) the largest stress magnitudes are observed to be those of S_{23} which shows a peak value of 0.692 MPa (Fig. 2e).

The magnitude of the stresses S_{11}, S_{22}, S_{33}, and S_{12} are observed to be comparatively negligible. Thus, the Mises stresses (Figs.2g-h) are observed to almost be entirely due the shear stress S_{23}. Stresses S_{11}, S_{22}, S_{33}, and S_{12} show localization near both ends. Figure 4 shows the sectional contour profiles for stresses S_{23} at z=147.8mm. Different length scale factors were adopted in generating the contour plots (i.e., the scale factor in the direction of the transverse direction is taken to be seven times larger than that in the lateral direction) for better visualization of the results. All stress fields except S_{13} are observed to be constant across the adhesive layer depth. Thus, for stress S_{13}, two contour plots are provided (Fig. 2f, i) to show the stress gradient across the thickness. Shear stress S_{13} is observed to range within $\pm$ 0.013 MPa and can thus be considered negligible compared to the stresses S_{23}. Two contour plots are provided for the von Mises stresses at the SA and AP interfaces (Figs.2g-h). Both figures are practically indistinguishable, suggesting that the von Mises stresses are nearly constant across the depth. The location of peak Mises is 1.20MPa and is found to occurs near the beam edges at z=147.8mm (Figs. 2g-h and Table 2).

For reference case R2, the distribution of stress fields S_{11}, S_{22}, S_{12}, and S_{13} (contours not shown) were observed to be similar to those of Case R1. Unlike Case 1, local peak Mises stresses were found to take place in two locations for Case R2 (Fig.3). The first local peak Mises stress is 2.18MPa (Table 2) and is located near mid-span (at z=2290.4mm). It is primarily due to a combination of the longitudinal stress S_{33} =1.138 MPa and shear stress S_{23}=1.073 MPa while the contributions of the other stresses to the Mises stress are found negligible. The second local peak Mises is analogous to that observed for the reference case R1. It is found to be 2.10MPa and is located near the beam edges (z=131.7mm). It is primarily due to the shear stress S_{23}=1.203 MPa. Table 2 provides the six stress components at the location of the peak von Mises stress S_M given by

$$S_M = \sqrt{\frac{1}{2}\left[\left(S_{11}-S_{22}\right)^2+\left(S_{22}-S_{33}\right)^2+\left(S_{11}-S_{33}\right)^2+6\left(S_{12}^{\;2}+S_{23}^2+S_{31}^2\right)\right]} \qquad (1)$$

Table 2. Stress field at the location of maximum Mises stress

Case		Stress (MPa)	S_{11}	S_{22}	S_{33}	S_{12}	S_{13}	S_{23}	S_M
Reference case 1 (z=147.8mm)			-0.008	-0.019	0.0090	-0.0003	-0.0015	0.692	1.20
Reference case 2	First Local peak Mises stress (z=2290 mm)		0.002	0.016	1.138	-0.0006	-0.0052	1.073	2.18
	Second local peak S_{23} stress (z=131.7mm)		0.004	0.019	0.064	-0.0018	-0.0059	1.203	2.08

For Case R1, by disregarding the stress component $S_{11}, S_{22}, S_{33}, S_{12},$ and S_{13} , and retaining the stress S_{23} , one obtains a Mises stress $S_M = \sqrt{3}S_{23} = \sqrt{3}S_{23} = \sqrt{3} \times 0.692 = 1.199 MPa$ which is 99.9% of the Mises stress including all six stress contributions. For Case R2, by disregarding $S_{11}, S_{22}, S_{12},$ and S_{13} and retaining the stresses S_{23} and S_{33}, one obtains a Mises stress $S_M = \sqrt{S_{33}^2 + 3S_{23}^2} = \sqrt{1.138^2 + 3 \times 1.073^2} = 2.18 MPa$, which equals the Mises stress within three significant digits including all six stress components. Thus, for all practical purposes, all but the shear stress S_{23} and S_{33} can be considered negligible when the adhesive is stiff (Ga=0.4GPa). Figure 4 depicts the stress distribution for shear stress S_{23} for the reference case R1 and shows that the stress gradient across the adhesive thickness is negligible. Also, Figure 5 is a schematic of the composite cross-section showing the location of the peak Mises stress.
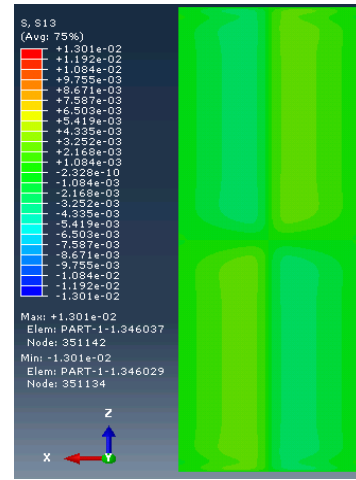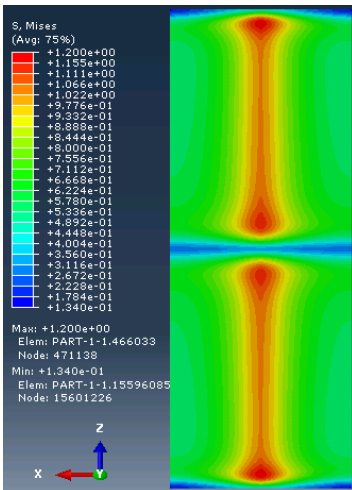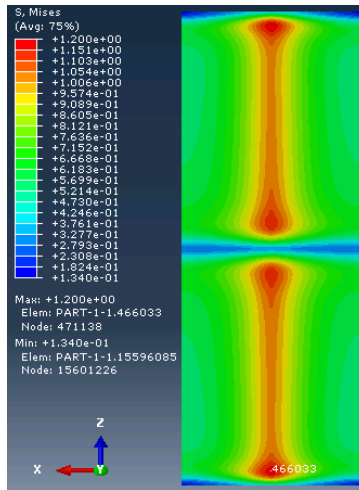

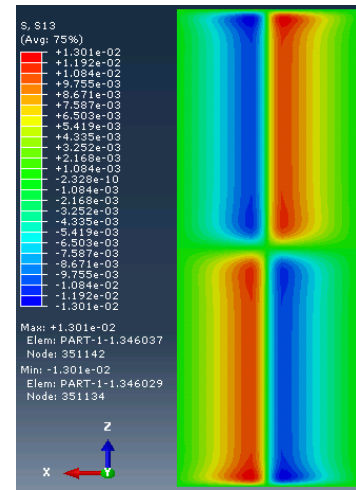(a) S_{11} (b) S_{22} (c) S_{33}
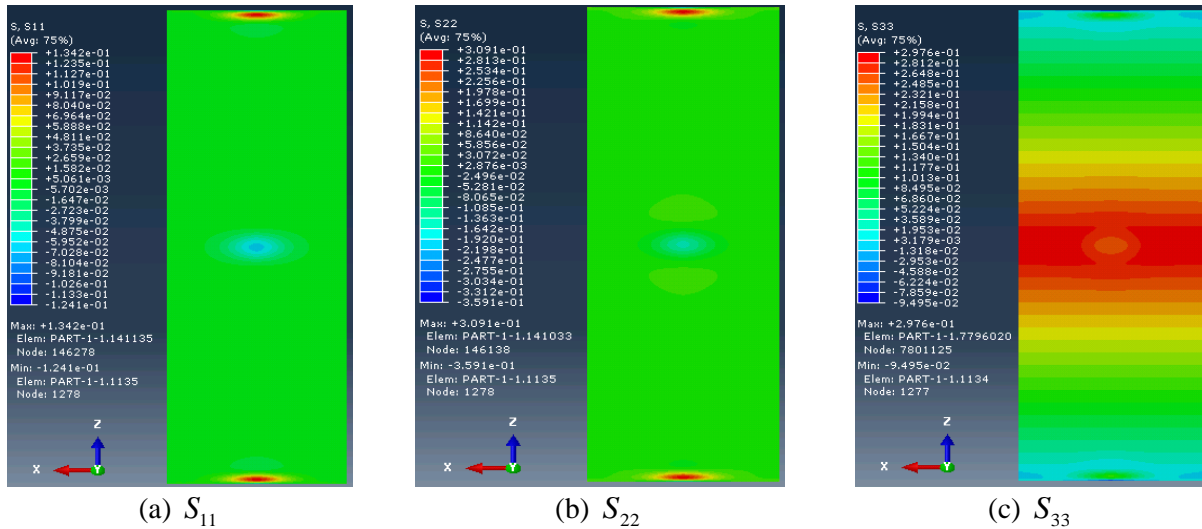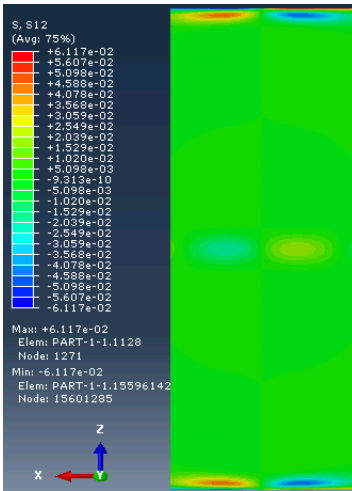
(d) S_{12}
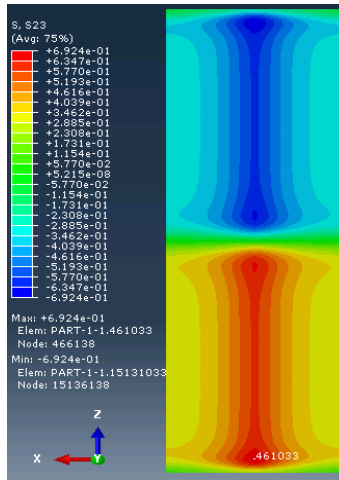
(e) S_{23}

(f) S_{13} - AP interface

(g) Mises stress-SA interface

(h) Mises stress -AP interface

(i) S_{13} - SA interface

Fig. 2. Plan view of the contours of stress fields at the adhesive-steel interface for reference case 1 (Length scale factor for X dimension =7).

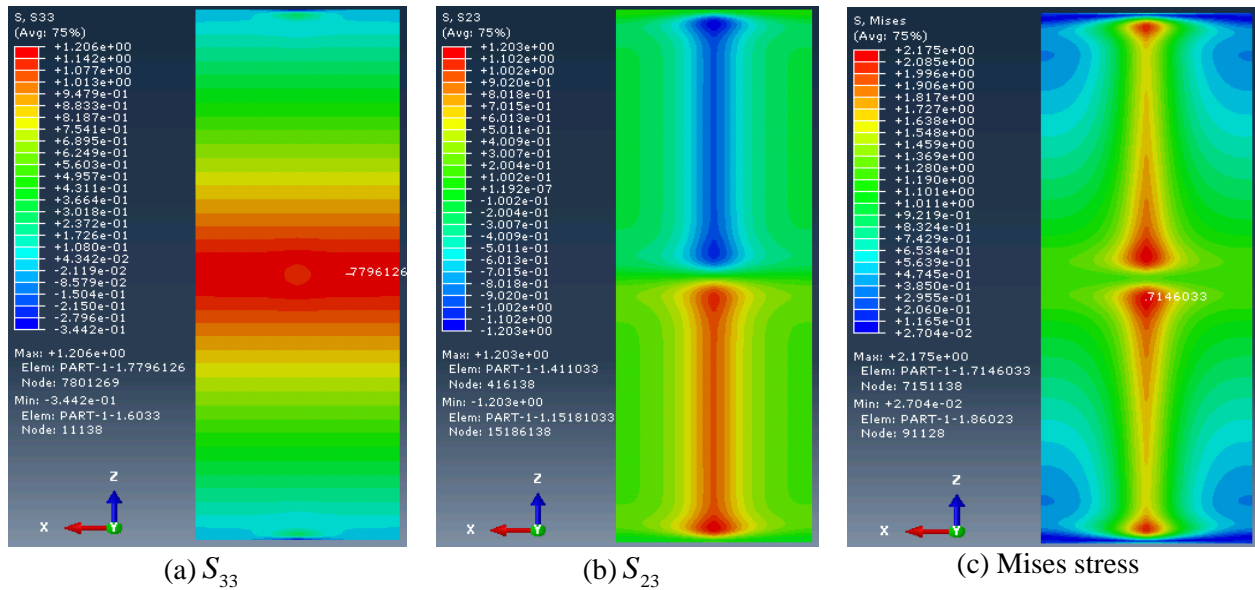(a) S_{33} (b) S_{23} (c) Mises stress

Fig. 3. Plan view of the contours of stress fields at the adhesive-steel interface for reference case 2 (Length scale factor for X dimension =7).

Fig. 4. Cross-sectional contour for shear S_{23} at z=147.8mm (reference Case R1) (Length scale factor for Y dimension =7)
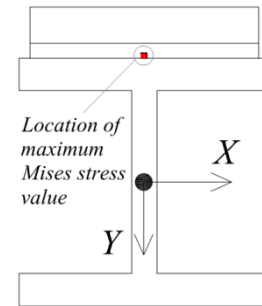
Fig. 5. Cross-section view

6. Transverse Normal Stresses

One of the failure modes observed when conducting ancillary tests to determine the adhesive properties (e.g., El Damatty and Abushagur (2003)) is the peeling mode of failure. When the GFRP plate is placed at the bottom of the beam as shown in Fig. 1b, the normal stress in the transverse direction S_{22} is predominantly compressive with a small localized tensile stress near the beam ends. The peak tensile stress in the region of localization is 0.309MPa. It is possible that the predicted localized tensile stress at the edge may be the cause of the experimentally observed peeling modes of failure. When the beam is reinforced by a GFRP plate placed at the top of the beam (Fig. 6a-R3), the stress S_{22} becomes predominantly tensile with the exception of the edges which are subjected to localized compressive stresses as shown in Fig. 6b, suggesting that the arrangement in Fig. 6a-R3 is more favourable than in Fig. 1a in terms of inducing a peeling failure. It is noted that the magnitudes of the stress S_{22} in both cases is identical while the sign is opposite. The magnitudes of the von Mises stresses in both cases are identical as evidenced by comparing Figs 2g and Fig. 6c.
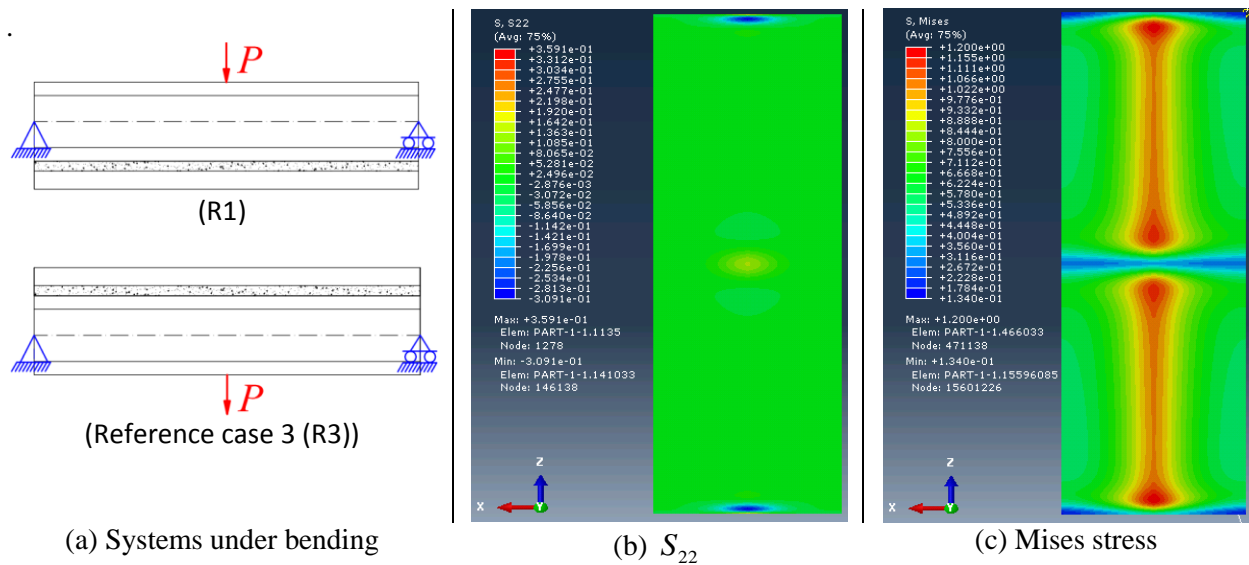
(a) Systems under bending   (b) S_{22} (c) Mises stress

Fig. 6. Steel beam-GFRP plate system under upwardly transverse loads

7. Parametric study

This section aims at investigating the effect of three parameters: the adhesive shear modulus, the adhesive thickness, and the GFRP plate thickness on the the peak transverse deflection as well as the peak stress S_{23}, peak stress S_{33} and von Mises stresses within the adhesive layer. Eighteen additional parametric runs were conducted by varying one parameter at a time. The matrix of parametric runs is presented in Table 3.

8. Effect of Shear Modulus

In runs 1 through 3, the shear modulus was varied from its value in the reference case. Figure 7 depicts the peak Mises stress in the adhesive versus the shear modulus of the adhesive. Also, depicted on the same plot is transverse deflection at the centroid of the mid-span cross-section versus the shear modulus in the adhesive. As the shear modulus of adhesive layer increases, the peak value of the von Mises stress is observed to increase. Conversely, an increase in the shear modulus of the adhesive is observed to correspond to a decrease in deflection as a result of the stronger interaction provided by the adhesive between the steel beam and the GFRP plate

The location of the peak Mises stress is observed to occur at the SA interface (Fig.5) for all adhesive shear modulus values.

Table 3. Parametric study

Case	G_a (MPa)	t_a (mm)	Ratio G_a/t_a (MPa/ mm)	t_p (mm)	Peak Stress within the adhesive layer (MPa)							mid-span deflection (mm)
					Location 1[1]				Location 2			
					von Mises	S_{23}	S_{33}	Coord. Z (mm)	von Mises	S_{23}	Coord. Z(mm)	
R1	100	2	50	19	Not needed for evaluation				1.20	0.69	147.8	19.79
R2	400	2	200	19	2.18	1.07	1.14	2290.4	2.08	1.20	131.7	19.77
1	5	2	2.5	19	Not needed for evaluation				0.72	0.42	200.7	20.06
2	50	2	25	19	As above				0.97	0.56	159.0	19.81
3	200	2	100	19	As above				1.57	0.90	139.8	19.78
4	400	0.5	800	19	As above				3.38	1.95	120.5	19.82
5	400	1	400	19	As above				2.70	1.56	125.3	19.81
6	400	2	200	19	2.18	1.07	1.14	2290.4	2.08	1.20	131.7	19.77
7	400	3	133	19	1.97	0.93	1.13	2288.8	1.78	1.03	136.6	19.74
8	400	4	100	19	1.85	0.85	1.13	2287.2	1.60	0.92	139.8	19.71
9	50	0.5	100	19	Not needed for evaluation				1.54	0.89	139.8	19.83
10	100	1	100	19	As above				1.55	0.90	139.8	19.82
11	200	2	100	19	As above				1.57	0.90	139.8	19.78
12	400	4	100	19	1.85	0.85	1.13	2287.2	1.60	0.92	139.8	19.71
13	400	2	200	10	1.83	0.74	1.30	2304.9	1.53	0.88	120.5	21.04
14	400	2	200	15	2.03	0.94	1.20	2295.2	1.87	1.08	126.9	20.32
15	400	2	200	25	2.38	1.24	1.05	2285.6	2.33	1.35	139.8	19.01
16	400	2	200	30	2.53	1.35	0.99	2280.8	2.49	1.44	144.6	18.4
17	400	2	200	35	2.67	1.45	0.93	2276.0	2.62	1.51	151.0	17.82
18	400	2	200	40	2.79	1.54	0.87	2271.2	2.73	1.57	155.8	17.28

*All peak Mises stresses are located at the steel adhesive interface
(1) Location 2 is for only cases that have the same response as Reference case 1 while locations (1) and (2) are for cases that have the same responses as Reference case 2.

9. Effect of Adhesive Thickness

In runs 4 through 8, the adhesive thickness was varied from its value in the reference case. Figure 8 depicts the peak Mises stress in the adhesive versus its thickness. Also, depicted on the same plot, is the transverse deflection at mid-span versus the thickness. As the thickness of adhesive layer increases, the peak value of the von Mises stress and the deflection are observed to decrease. In all cases, the location of the peak Mises stress is observed to take place only at the SA interface (Fig.5) and to gradually move towards to the bottom beam end edge when the adhesive thickness increases.

For the cases 4 and 5, it is observed that the peak von Mises stress occurs near the beam ends. When the thickness of the adhesive layer is great enough (≥ 2 mm), the longitudinal normal stress within the adhesive layer and at the mid-span area contributes a considerably to the von-Mises stress.
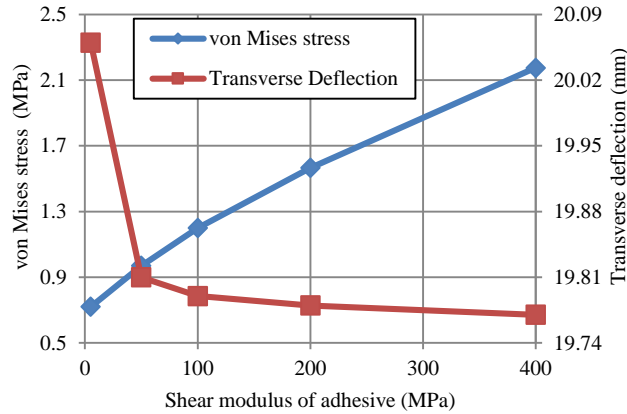
Fig. 7. Relationship between shear modulus of adhesive layer to von Mises stress and transverse deflection at mid-span
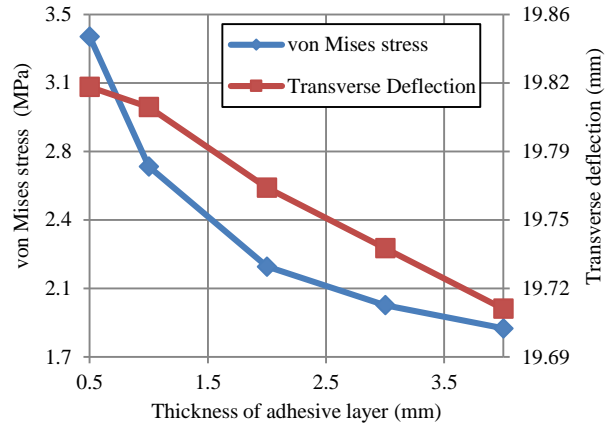
Fig. 8. Relationship between thickness of adhesive layer to Von Mises stress and transverse deflection at mid-span

10. Effect of the G_a / t_a Ratio

In the work of Pham and Mohareb (2014 a, b), it was observed the total strain energy within the adhesive layer remains essentially unchanged when the adhesive thickness t_a is small and the ratio G_a / t_a is kept constant, i.e., the degree of interaction between steel beam and GFPR plate remained essentially unchanged for a given G_a / t_a value. A similar observation is made when examining runs 9-11 which give essentially the mid-span deflection, while run 12 for which $t_a = 4mm$ predicted a small reduction in the transverse deflection at mid-span.

11. Effect of GFRP Plate Thickness

In runs 13 through 18 of Table 3, the GFRP plate thickness was varied from its value in the reference case. The location of the peak von Mises stress is observed to be farther from mid-span when the GFRP plate thickness increases (Table 3). Across the height, the peak Mises stress is observed to occur either at the SA interface. Figure 9 depicts the peak Mises stress in the adhesive versus the thickness of the GFRP plate. Also, depicted on the same plot is the transverse deflection at mid-span versus the thickness. As the thickness of the GFRP plate increases, the transverse deflection at mid-span is observed to gradually decrease while the von Mises stress increases. A thicker GFRP plate is observed to be associated with two benefits: a) a decrease in the deflection of the beam and b) a decrease in the von-Mises stress in the adhesive.
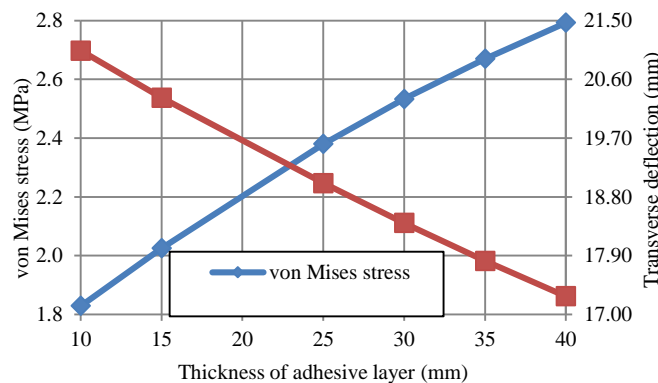

Fig. 9. Relationship between thickness of adhesive layer to Von Mises stress and transverse deflection at mid-span

12. Conclusions

Based on the present study on a composite beam under concentrated loads applied at mid-span, the following conclusions can be drawn:

1. The most predominant stress field within adhesive layer is the shear stress S_{23} for low shear modulus ($\leq 200 MPa$) and thin adhesive layer ($\leq 1mm$). It is found to be responsible for 99.9% of the von Mises stress. For higher values of the adhesive shear modulus and/or thickness, the predominant stress fields are S_{33} and S_{23}.

2. The five stress fields $S_{11}, S_{22}, S_{33}, S_{12}, S_{23}$ and the von Mises stress are observed to be nearly constant across the adhesive thickness. In contrast, the shear stress S_{13} is observed to have a slight gradient across the thickness.

3. The peak Mises stresses are observed to occur at the middle fibers of steel-adhesive interface, and are located at the edges and at mid-span.

4. An increase in the shear modulus of adhesive corresponds to an increase in the von Mises stress within adhesive layer and a decrease of mid-span deflection. In such cases, the location of peak von Mises stress becomes closer to the beam end edge.

5. When the thickness of adhesive layer is small (<2mm), the von Mises stress and transverse deflection at mid-span are observed to remain almost unchanged when the ratio shear modulus/thickness of adhesive layer is kept constant.

6. When the GFRP thickness is increased, the mid-span displacement decreases. This beneficial effect is offset by the fact that the Mises stresses within the adhesive increase, potentially leading to adhesive failure.

References

El Damatty, A.A. and Abushagur, M. (2003), Testing and modeling of shear and peel behavior for bonded steel/FRP connections, Thin-Walled Structures, 41(11), 987-1003.

El Damatty, A., Abushagur, M. and Youssef, M. A. (2003), Experimental and analytical investigation of steel beams rehabilitated using GFRP sheets, Journal of Steel & Composite Structures 3(6), 421-438.

Linghoff, D. and Al-Emrani, M. (2010), Performance of steel beams strengthened with CFRP laminate – Part 2: Laboratory tests, Composites Part B, 41(7), 516-522.

Miller, C.T., Chajes J.M. and Hastings N.J. (2001), Strengthening of a steel bridge girder using CFRP plates, Journal of Bridge Engineering 6(6), 514-522.

Peiris, N.A. (2011), Steel Beams Strengthened with ultra High Modulus CFRP Laminates, Doctoral Thesis, College of Engineering, University Kentucky.

Pham, P.V. and M. Mohareb (2014), A shear deformable theory for the analysis of steel beams reinforced with GFRP plates, Thin Walled Structure, 85, 165-182.

Pham, P.V. and M. Mohareb (2014), Finite-Element Formulations for the Spatial Static Response of Steel Beams Bonded to a GFRP Plate, Journal of Engineering Mechanics, 10.1061/(ASCE)EM.1943-7889.0000862, 04014143.

Schnerch, D., Dawood, M., Rizkalla, S., Sumner, E. and Stanford, K. (2005), Bond behavior of CFRP strengthened steel structures, Advances in Structural Engineering, 9(6), 805-817.

Siddique, M.A.A. and El Damatty, A.A. (2013), Improvement of local buckling behaviour of steel beams through bonding GFRP plates, Composite Structures, 96(6), 44-56.

Xia, S.H. and Teng, J.G., Behaviour of FRP-To-Steel Bonded Joints, Proceedings of International Symposium on Bond Behaviour of FRP in Structures, 2005, 411-418.